A 403 MHz Wireless Power Transfer System with Tuned Split-ring Loops for Implantable Medical Devices

Jingchen Wang, Eng Gee Lim, Mark Paul Leach, Zhao Wang, Rui Pei, Zhenzhen Jiang, and Yi Huang

***Abstract*—A near-field wireless power transfer (WPT) system for implantable medical devices such as pacemakers is proposed. Operating at 403 MHz within the Medical Implants Communication Service (MICS) band, the WPT link constitutes a primary loop to be based outside the body as a transmitter and an implantable loop with a single turn as a receiver. Simulation and experimental results show that the proposed link offers good power transfer efficiency performance. The maximum measured power transfer efficiency of the proposed link is 57.9% at a transfer distance of 6 mm through 1 mm of air and 5 mm of body tissue. The maximum input power that can be supplied to stay within specific absorption rate safety guidelines is 159 mW. A rectifying circuit is designed to convert 403 MHz RF signals to DC for a 1.5 kΩ load with a measured conversion efficiency of 73.2%. The measured end-to-end power transfer efficiency of the proposed wireless power transfer system is 42.4%.**

***Index Terms*—Wireless power transfer, split-ring loops, near-filed, magnetic resonance coupling, implantable medical devices.**

I. Introduction

CONVENTIONAL implanted electronic devices rely heavily on continuous power supplied by batteries, typically designed to provide energy for no more than 12 years [1]. To supply energy or replenish depleted implanted power sources for implantable medical devices (IMDs) such as pacemakers [2-4], wireless capsule endoscopes [5,6] and neural implants [7,8], a reliable and convenient method is vital. Wireless power transfer (WPT) technology, in which radiated electromagnetic waves are used to convey power from one location to another, is of increasing interest to the scientific community. It can be applied in applications [9-13] where it is not feasible to provide continuous power to devices, powering them wirelessly and hence overcoming battery life limitations and avoiding umbilical cables. With the aid of WPT technology, surgeries for replacing batteries can be avoided, hence associated health risks, patient inconvenience and economic burden can also be mitigated [14].

Far-field (radiative) and near-field (non-radiative or coupled-based) approaches are the two main directions of WPT techniques. Far-field approaches have advantages over near-field approaches such as longer transfer distances and a relaxed transmitter/receiver alignment tolerance. However, the overall power transfer efficiency (PTE) of far-field approaches is low and the requirements on safety are high [15]. An implantable rectenna, including a miniaturized planar inverted-F antenna (PIFA) with a folded ground and a rectifier circuit, is proposed in [15]; operating at 2.45 GHz in the far-field over a distance of 0.5 m it can receive −11 dBm of power. The large free space path loss over such a distance at this frequency and low power density due to spreading of the radiated power results in a measured PTE of less than 0.001%. Additionally, RF-to-DC converters typically have a low efficiency at low power levels, for example, a conversion efficiency of 15.7% was achieved at an input power of −20 dBm in [16]. In view of the low PTE and low RF-DC conversion efficiency for a far-field system, to supply sufficient power to an implantable device the transmit power needs to be increased. However, there are limits on the maximum transmitting power for an implanted antenna set by the Federal Communications Commission (FCC) [17] due to safety considerations. Therefore, although far-field WPT can operate over a longer transfer distance than near-field WPT, due to the low power density, low transit efficiency, and restrictions on transmit power, the power received by the implanted antenna is limited.

Magnetic resonance coupling (MRC), as one of three near-field WPT mechanisms [18] (MRC, inductive coupling, and capacitive coupling), has increasingly attracted researchers for implantable applications, as it can offer a higher power transfer efficiency over larger transfer distances than inductive or capacitive coupling methods [19]. Examples of this have been published working at less than 15 MHz [20-22], chosen due to the low specific absorption by body tissues. However, the wire coils proposed occupy a significant amount of the implant space, exacerbating the inconvenience of their operation. Circular printed spiral coils (PSCs) are proposed in [23] and tested using

This work is partially supported by the AI University Research Centre (AI-URC) through XJTLU Key Programme Special Fund (KSF-P-02) and XJTLU Research Development Fund (PGRS-13-03-06, RDF-14-03-24, RDF-14-02-48, PGRS 2006007 and PGRS 2012013).

Jingchen. Wang, Eng. Gee. Lim, Mark. Leach, Zhao. Wang, Rui. Pei and Zhenzhen. Jiang are with the School of Advanced Technology, Xi'an-jiaotong Liverpool University, Suzhou 215123, P. R. China. Yi. Huang is with the Department of Electrical Engineering and Electronics, The University of Liverpool, Liverpool L69 3BX, U.K. (correspondence e-mail: mark.leach@xjtlu.edu.cn).

a beef muscle tissue environment over a transfer distance of 10 mm. A measured PTE of 35.4% was achieved at a resonance frequency of 13.56 MHz. An operating frequency of 60 MHz was used for mm-sized implants over a transfer distance of 16 mm in [24] though a measured PTE of only 2.4% was achieved. As the operating frequency increases, the power transfer efficiency of the WPT link significantly decreases. For a biomedical capsule endoscope, a wearable multi-coil resonance wireless power transfer system operating at 0.25 MHz achieved a measured PTE of 5.4% [25]. However, these coils generally require a complex matching circuit to convert RF energy to DC power, decreasing the overall power transfer efficiency and hence received power. In addition, for circuit simplification planar coils are easier to be integrated with a rectifying circuit than coils made from copper wire.

This work presents an efficient wireless power transfer system for implantable applications working at an operating frequency of 403 MHz, which belongs to the Medical Implants Communication Service (MICS) band from 402 MHz - 406 MHz and is licensed for implantable devices. For WPT into dispersive body tissues, when transmit antennas have dimensions on the order of centimeters, the optimal frequency is in the sub-GHz region since power gain increases with the frequency; whereas it decreases significantly with frequency in the GHz region where dielectric loss dominates [26]. When the dimensions are on the order of centimeters, the peak of the power gain occurs in the sub-GHz region because the induced current loss of coils still dominates, whereas the peak of the power gain occurs in the GHz region when dimensions are on the order of millimeters because dielectric loss dominates.

To be integrated easily, coils with a planar structure for WPT can be realized in the ultra-high frequency band as well as with a smaller dimension. Multiple split-ring loops are used to enhance the magnetic density at high frequency. A lumped capacitor is used to decrease the resonant frequency significantly, leading to the formation of an intrinsic-resonator with series inductor-capacitor (*LC*) characteristics. The power transfer efficiency of the proposed WPT system is not sensitive to detuning of the operating frequency due to environmental conditions or manufacturing tolerances. The system is designed to maximize transfer efficiency at the maximum allowable transmit power based on Specific Absorption Rate (SAR) regulations, which maximizes power delivery and hence could shorten the charging time for a battery.

The paper is organized as follows. The design principles of the transmit (Tx) and receive (Rx) loops are presented in Section II. The performance of the proposed WPT link between the Tx and Rx loops including the influences of lateral and angular misalignments on WPT efficiency are considered in Section III. The measurement setup and measured results of the proposed WPT link are illustrated in Section IV. The performance of the designed RF to DC rectifier is shown in Section V. The measurement setup and measured results of the proposed WPT system are depicted in Section VI. Finally, conclusions are provided in Section VII.

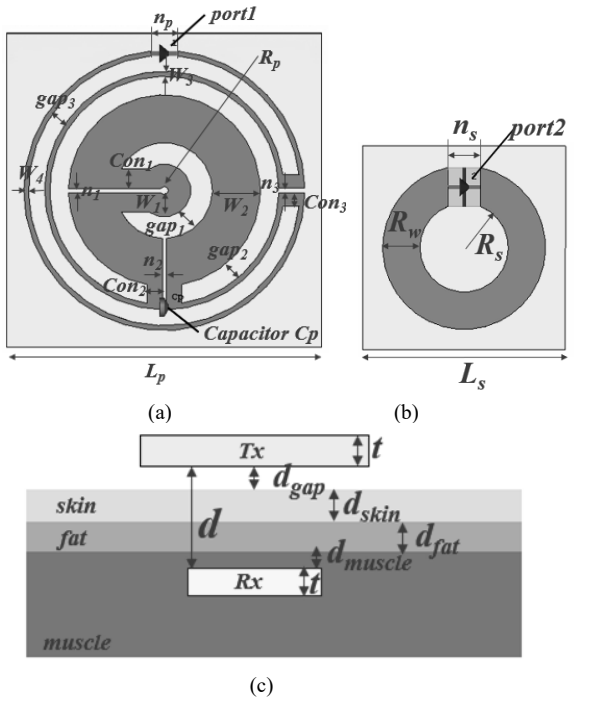

Fig. 1. Physical layout models of (a) Tx loop; (b) Rx loop; (c) Configuration of the proposed WPT Link.

TABLE I. Characteristics of human tissues used at 403 MHz for the simulation

Tissues	ε_r	σ (S/m)	Average ρ (kg/m^3)
Skin (Dry)	46.7	0.689	1090
Fat	11.6	0.0808	1109
Muscle	57.1	0.797	911

TABLE II: DIMENSIONS OF THE PROPOSED LOOPS (UNITS: mm)

Parameter	Value	Parameter	Value
L_p	39.6	L_s	25.5
n_p	3.3	n_s	4.08
Rp	0.5	R_s	5.56
W_1	2.84	R_w	4.67
W_2	6.04	*d*	6
W_3	0.64	t	1.5
W_4	0.6	d_{gap}	1
gap1	2.72	d_{skin}	2
gap2	2.34	d_{fat}	2
gap3	2.02	d_{muscle}	1
n	0.55		
Con1	2.47		
Con2	1.91		
Con3	1.67		

II. DESIGNS PRINCIPLES OF THE TRANSMITTER AND RECEIVER

To maximise the magnetic resonance power available for WPT at high frequency (hundreds of Mega-Hertz), a multiple split-ring loop is used to replace the traditional printed spiral coil. This loop is placed in parallel with a lumped element capacitor *Cp* (as shown in Fig. 1(a)) to form a series resonator with an intrinsic resonance frequency of 403 MHz for use as the transmitting resonator. The schematic of the Tx resonator is shown in Fig. 1 (a). The retuned split-ring loop has been

This article has been accepted for publication in a future issue of this journal, but has not been fully edited. Content may change prior to final publication. Citation information: DOI 10.1109/TAP.2021.3111520, IEEE Transactions on Antennas and Propagation

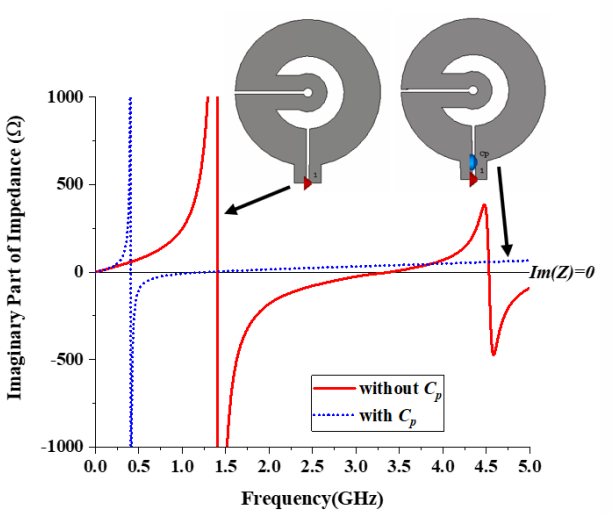

Fig. 2. The imaginary part of impedance of two split-ring loops without and with a lumped element capacitor.

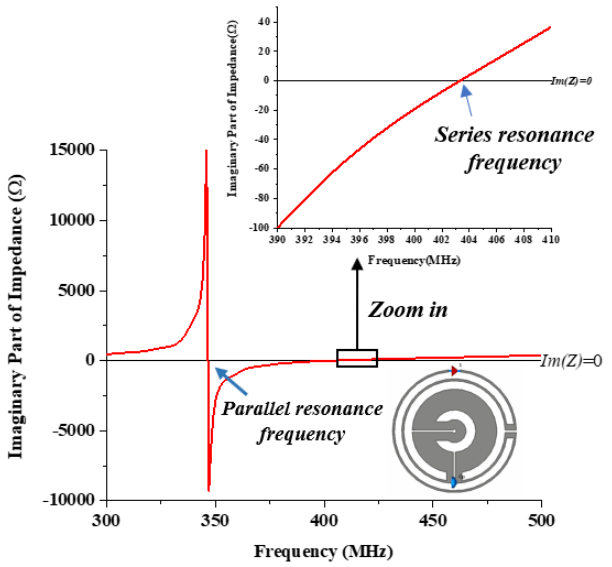

Fig. 3. The imaginary part of impedance of final designed primary loops.

designed using the roundabout technique on FR-4 substrate (with a relative dielectric constant ε_r=4.4). The Tx resonator will be located outside of the body during system operation. To realize miniaturization and simplification, the Rx loop is a single turn loop with a diameter of 20.46 mm^2, as shown in Fig. 1 (b) and is printed on a square FR-4 substrate of 25.5 mm^2 and height of 1.5 mm. This is small enough to be housed within most standard pacemakers which are on the order of 41.2 mm×41.5 mm [27].

Normally, pacemakers are implanted under the chest skin area [28], the thickness of skin on the human body is 0.5 mm ~ 4.0 mm [29]. The distance between Tx and Rx for the purposes of simulation is considered to be 6 mm, which is larger than the thickness of human skin. The localized body is modelled as a typical set of planarly layered mediums at a pacemaker implant site, consisting of skin, fat and muscle. The distance between Tx and Rx is modelled to include an air gap of 1 mm and then

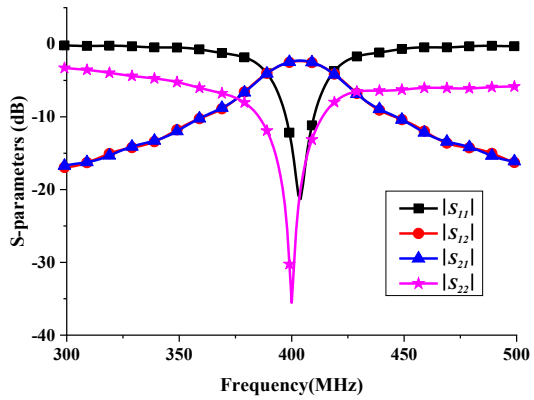

Fig. 4. The simulated S-parameters of proposed WPT link for wireless power transfer.

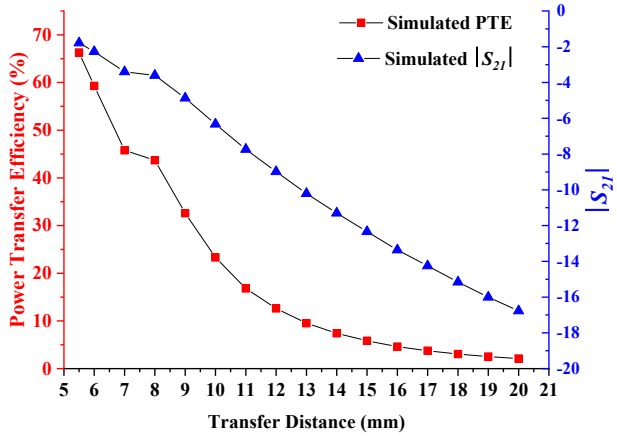

Fig. 5. The simulated transmitting parameter and link power transfer efficiency between two proposed loops for wireless power transfer against the transfer distance between Tx and Rx loops.

skin, fat, and muscle at 2 mm, 2 mm and 1 mm, respectively as shown in Fig. 1 (c). According to the IT'IS Foundation database [30], the relative permittivity, conductivity, and mass density of skin, fat, and muscle at 403 MHz are listed in TABLE I.

All parameters of the Tx and Rx loops have been optimized by means of full-wave simulations performed using the transient solver of CST Microwave Studio and using the body tissue model shown in Fig. 1(c).

The final physical layout of the designed loops and the placement of the loops with respect to the body tissue are shown in Fig. 1 (c). The details of the optimized parameters for the loops are provided in TABLE II. The capacitance of the lumped element capacitor (*Cp*) used in the Tx resonator is 7.9 pF.

Generally, a series resonating circuit is used at the transmitting side for wireless power transmission [31]. The impedance characteristics of a traditional parallel intrinsic-resonating circuit have a zero crossing that changes from inductive to capacitive, whereas for a series intrinsic-resonating circuit the change is from capacitive to inductive [32]. Therefore, in designing the series resonator for the transmit side of the system, the imaginary part of the impedance should change from negative to positive (i.e. from capacitive to inductive) and be zero at the required resonance frequency (403 MHz).

This article has been accepted for publication in a future issue of this journal, but has not been fully edited. Content may change prior to final publication. Citation information: DOI 10.1109/TAP.2021.3111520, IEEE Transactions on Antennas and Propagation

The trends of the imaginary part of the impedance with and without the compensation capacitor are illustrated in Fig. 2. Without the capacitor the two inner split-ring loops of the Tx loop have a series intrinsic-resonance of around 3.39 GHz, which is much larger than the desired frequency of 403 MHz. When the parallel lumped element capacitor is introduced, it increases the equivalent overall capacitance, which in turn decreases the resonance frequency. The lumped element capacitance is chosen as 7.9 pF, which decreases the series resonance frequency to 1.3 GHz. Finally, two extra loops were added to the outside of the design for the optimization of WPT link, as shown in Fig. 1(a). One the one hand, the aim is to decrease the series resonance frequency slightly and realise the impedance matching at 403 MHz. On the other hand, the inductance of Tx loop is optimized to enhance the power transfer efficiency of the WPT link. The imaginary part of the final resonator impedance is shown in Fig. 3. The parallel resonance frequency is seen to be around 348 MHz. As frequency increases beyond this point the impedance increases to a capacitive maximum and then gradually decreases again. At 403 MHz, the impedance changes from capacitive to inductive, characterising a series resonant frequency and hence looks like a series *LC* circuit, suitable for use as the primary WPT circuit resonator.

The receiving loop exhibits a parallel *LC* circuit characteristic at 403 MHz and hence the combination constitutes a series-primary parallel-secondary WPT link.

III. The Performance of the Proposed WPT Link

A. The Performance of Wireless Power Link

Fig. 4 shows the S-parameters obtained through simulation of the structure described in Fig. 1(c). A reference impedance of 50 Ω has been used at both ports. It can be seen from Fig. 4 that the proposed resonator operates at 403 MHz with a bandwidth of at least 13 MHz (397-410 MHz) for S_{11}<−10 dB, which covers the 402-405 MHz MICS band. Additionally, at 403 MHz, the scattering parameters are $|S_{11}|$=−20.8 dB, $|S_{21}|$=−2.27 dB, and $|S_{22}|$=−22.24 dB.

To conduct practical measurements of power transmission, assuming that both source impedance (R_{in}) and load impedance (R_L) are 50 Ω, the link power transfer efficiency ($\eta_{RF\text{-}RF}$) between the proposed Tx-Rx loops can be defined as [33]:

$$\eta_{RF-RF} = \frac{P_{receiving}}{P_{transmitting}} = \frac{Power\ delivered\ to\ the\ receiver}{Available\ power\ from\ the\ source} = |S_{21}|^2 \times 100\% \quad (1)$$

The trends of the simulated link power transfer efficiency (PTE) and transmission parameter ($|S_{21}|$) against the transfer distance between Tx and Rx loop as the Rx is moved deeper into the muscle layer is shown in Fig. 5. It can be seen that the link PTE decreases as the implanted depth increases. The link PTE is 66.28% ($|S_{21}|$=−1.786 dB) at a transfer distance of 5.5 mm (i.e. at a secondary resonator implant depth of 4.5 mm), whereas it decreases to 2.03% ($|S_{21}|$=−16.93 dB) when the transfer distance increases to 20 mm. The link PTE remains over 40% for transfer distances between 5.5 mm and 8 mm.

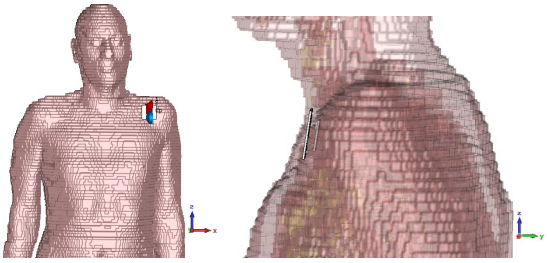

(a) (b)

Fig. 6. The schematic of the Gustav model with the proposed WPT link (a) front view; (b) side view.

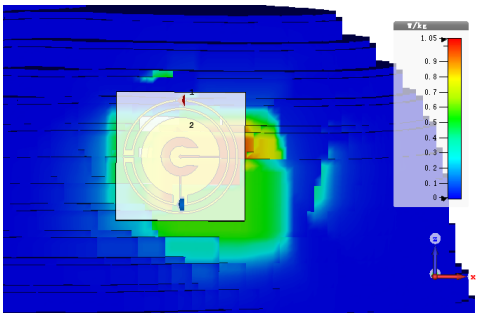

Fig. 7. SAR distribution of the proposed WPT link at 403 MHz averaged 10-g tissue.

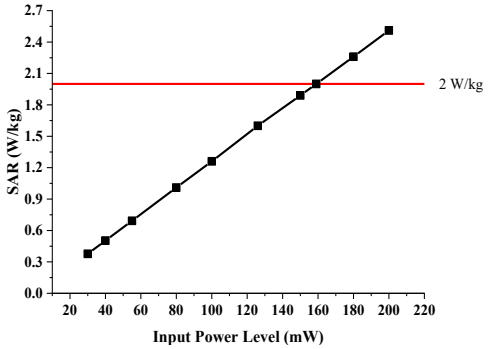

Fig. 8. The trend of calculated 10-g average SAR value with different input power level. The SAR limit (2 W/kg) is plotted as the horizontal line.

B. SAR Evaluation

According to the IEEE C95.1-2005 standards on human safety, the 10-g average SAR should be less than 2 W/kg [34]. Full-wave simulations were performed using CST Microwave Studio to obtain the SAR value. The Gustav model was used, together with the WPT link, as shown in Fig. 6. The segmentation of transmit loop can significantly decrease the SAR value [35], the SAR distribution averaged over 10-g of this proposed WPT link at 403 MHz is reduced, as shown in Fig. 7. To determine how much power can be provided to the primary resonator of the proposed WPT link based on these safety regulations, the trend of the SAR value against primary resonator input power is given in Fig. 8. The horizontal line represents the 10-g average SAR limitation of 2 W/kg and the black line shows the calculated SAR value for this WPT link in body tissue. The calculated SAR value is directly proportional to the input power delivered to the primary resonator. To satisfy the IEEE SAR regulations (2 W/kg), the input power delivered to the primary resonator should be less than 159 mW at 403 MHz.

This article has been accepted for publication in a future issue of this journal, but has not been fully edited. Content may change prior to final publication. Citation information: DOI 10.1109/TAP.2021.3111520, IEEE Transactions on Antennas and Propagation

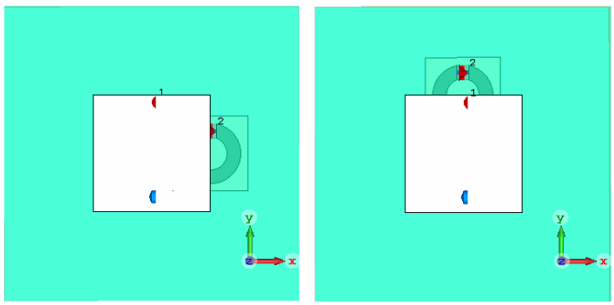

(a) (b)

Fig. 9. The case of misalignment due to a shift along with (a) x-axis and (b) y-axis.

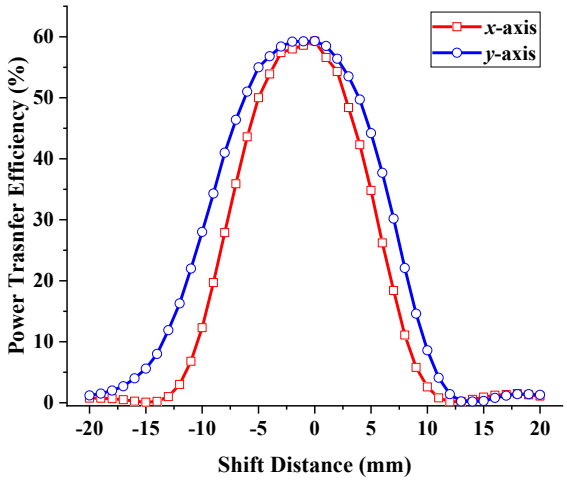

Fig. 10. The simulated link power transfer efficiency against a shift distance along with *x*-axis and *y*-axis.

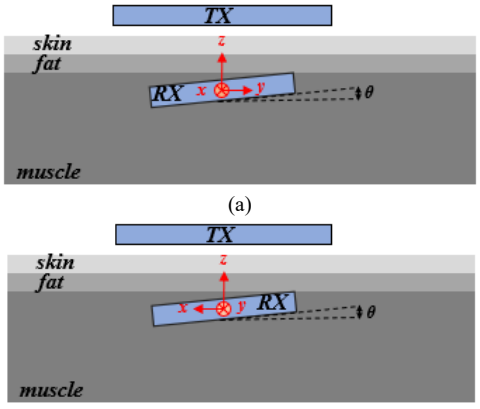

Fig. 11. The case of misalignment due to a rotation of the Rx loop in the (a) *yz*-plane and (b) *xz*-plane.

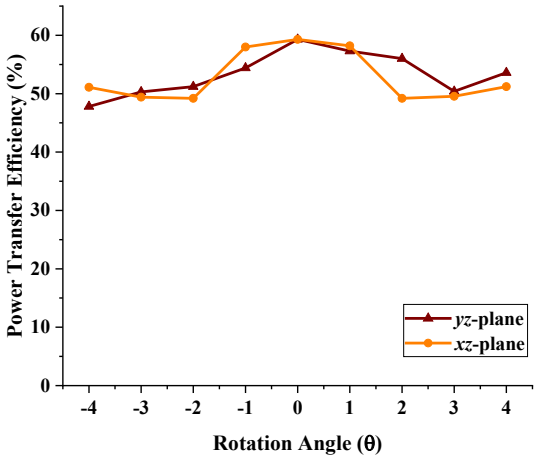

Fig. 12. The simulated link power transfer efficiency against rotation angle in the *yz*-plane and *xz*-plane.

C. *Misalignment Analysis*

In practice, the Rx loop is implanted in the muscle and the Tx loop sits on the surface of the body. It is unlikely that they will be perfectly aligned. There may exist small lateral shifts in *x* or *y*. Therefore, it is necessary to investigate the effect of plane misalignment on link PTE. Fig. 9 shows simulations of misalignment in both the *xz* and *yz* planes.

The trends of link PTE against shift distance along each of the principal planes are shown in Fig. 10. Misalignments of up to 3 mm have little influence on the link PTE. However, the link PTE declines rapidly as the shift value increases beyond 5 mm. The link PTE remains over 50% for shifts in the *xz*-plane from -5 mm to 3 mm for shifts in the *yz*-plane from -6 mm to 4 mm.

Misalignment may also occur due to off-boresight rotation of the loops. This may happen due to inaccurate placement of the Rx loop during surgery. The Rx loop is implanted in muscle at a depth of 1 mm, based on the board size the maximum possible angle of rotation is ±4°. Misalignments due to a rotation of the Rx loop in each plane are shown in Fig. 11. The trends of link PTE against rotation angle in different planes are illustrated in Fig. 12.

It can be seen from Fig. 12 that link PTE decreases gently from 59.3% to 47.8% as the absolute value of rotation angle in each of the two planes increases from 0° to 4°. In the *yz*-plane, the distance between the two discrete ports enlarges as the rotation angle increases from −4° to 4°, which results in a larger link PTE for positive rotation angles than for negative rotation angles. In the *xz*-plane, the distance between the two discrete ports is symmetrical with varying rotation angle, resulting in a symmetrical trend in link PTE. Considering the edge of the Rx loop is almost in the fat tissue layer at a rotation angle of ±4°, the lower permittivity and conductivity of the fat leads to a small increase in link PTE at these extremes. In general, the rotation angle has little influence on WPT link performance.

Overall, both lateral misalignments within the range ±5 mm and angular misalignments up to ±4° have little influence on the performance of this proposed implantable WPT link.

D. *The Influence of the Pacemaker Case*

As pacemaker cases are typically made of titanium [36], it is necessary to investigate the influence of the metallic pacemaker case on the performance of the proposed WPT link. In terms of efficiency, it is better to place the WPT secondary loop outside the metallic case of the pacemaker, which is not easily penetrable by electric and magnetic fields [37]. The configuration of the proposed WPT link in the presence of the pacemaker case is shown in Fig. 13(a). The pacemaker case has been modeled as a simple elliptical cylinder enclosure with

This article has been accepted for publication in a future issue of this journal, but has not been fully edited. Content may change prior to final publication. Citation information: DOI 10.1109/TAP.2021.3111520, IEEE Transactions on Antennas and Propagation

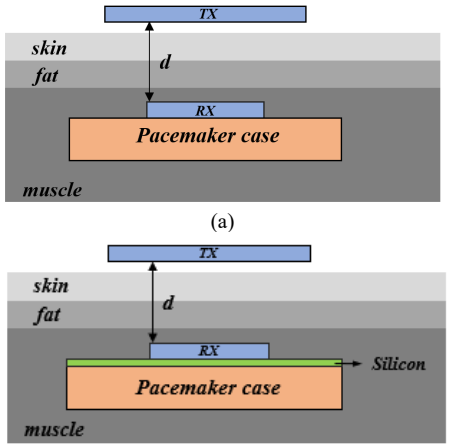

Fig. 13. The configuration of the proposed WPT link in the present of (a) pacemaker case; (b) pacemaker case and silicon.

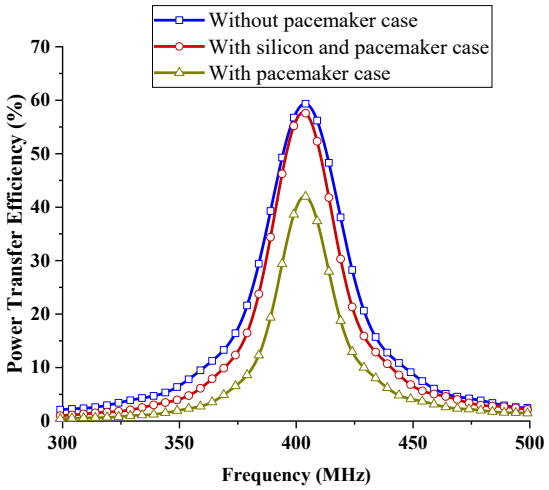

Fig. 14. The simulated link power transfer efficiency in different cases.

external radii of 30 mm and 25 mm and a height of 10 mm. The materials are titanium alloy with a wall thickness of 1 mm.

The link PTE in the presence of the case is depicted in Fig. 14. It is can be seen that the link PTE at 403 MHz is affected by the metallic pacemaker case and decreases to 42%. The reason for this is that the magnetic field produced by the proposed WPT link generates eddy currents in the metallic case modifying the magnetic field behavior and, consequently, the values of the self-inductance and mutual inductance of the loop [37].

To prevent the proposed WPT link from the effects of the pacemaker case, a thin layer of silicon, 1 mm, is inserted between the WPT secondary loop and the pacemaker, as illustrated in Fig. 13(b). From Fig. 14, the link PTE with the added silicon layer is 57.7% at the operating frequency. In this case, the metallic pacemaker case has little influence on the performance of the proposed WPT link.

IV. Measurement of the Proposed WPT Link

A. Measurement Setup

The proposed Tx and Rx loops were fabricated on FR-4 substrate as shown in Fig. 15(a). Fig. 16(b) shows the

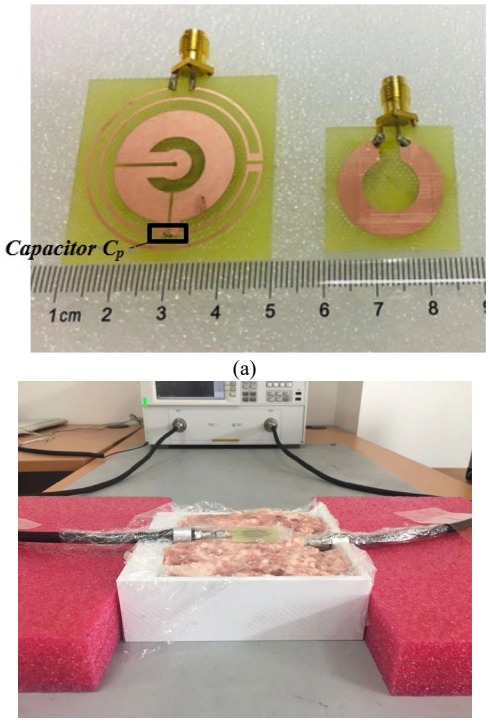

Fig. 15. (a) Fabricated antennas; (b) Measurement of proposed loops for wireless power transfer.

measurement setup, where a calibrated N5230C Vector Network Analyzer (VNA) from Keysight is used with a reference impedance of 50 Ω. The two loops are directly soldered to subminiature version A (SMA) connectors and then connected to the two VNA ports, respectively. The Rx loop is placed inside some minced pork, used to simulate the body tissue, and the Tx loop is put on the surface of the minced pork. Both loops and connectors are protected by a thin layer of plastic wrap. As the effects of the pacemaker case have been shown to be mitigatable, it is not included for the purposes of measurement.

B. Experimental Results and Comparisons

Comparisons of the measured *S*-parameters with simulations are shown in Fig. 16. A small frequency shift is seen to exist between the simulation and measurement results. The value of S_{11} is below -10 dB from 394 MHz to 406 MHz, covering the entire MICS band. At 403 MHz, the values of measured $|S_{11}|$, $|S_{21}|$, $|S_{22}|$ are -12.4 dB, -2.37 dB and -10.8 dB, respectively. Overall, the measured results show good agreement with the simulated results.

The calculated and measured link PTE for the system are shown in Fig. 17. Good agreement is seen between the simulated and measured link power transfer efficiencies despite the slight frequency shift. The simulated link PTE reaches a peak of 59.3% at 403 MHz, whereas the maximum measured link PTE is 60.7% at 400 MHz. The measured link PTE remains at over 50% over a bandwidth of 17 MHz (from 390 MHz to 407 MHz). Therefore more than half of the transmit power is received by the receiving loop despite the shift in resonating frequency. The link PTE dramatically decreases to 20% from

This article has been accepted for publication in a future issue of this journal, but has not been fully edited. Content may change prior to final publication. Citation information: DOI 10.1109/TAP.2021.3111520, IEEE Transactions on Antennas and Propagation

TABLE III: COMPARISONS OF THIS PROPOSED WPT LINK WITH OTHER WORK

Ref.	Types	f_0 (MHz)	Tx Size (mm)	Rx Size (mm)	Transfer Distance (mm)	Simulated $\|S_{21}\|$ /Link PTE (%)	Measured $\|S_{21}\|$ /Link PTE (%)	Maximum Source Power (mW)	Maximum Receiving Power (mW)
[38]	Wire coils	5	70×70	35×35	20	82%	80%	/	18
[39]	Dual-band Antenna	13.56	85×85	25×25	16	/	17%	100	17
[40]	Square Coils with Metamaterials	430	40×40	10×10	20	−15.4dB/2.88%	−16dB/2.51%	/	/
[41]	Planar Ring Resonator	403	20.48×20.48	15.48×15.48	5	−6.83dB/20.75%	−6.87dB/20.54%	38	7.77
This work	Planar Tuned Split-ring loops	403	39.6×39.6	25.5×25.5	6	−2.27dB/59.3%	−2.37dB/57.9%	159	92

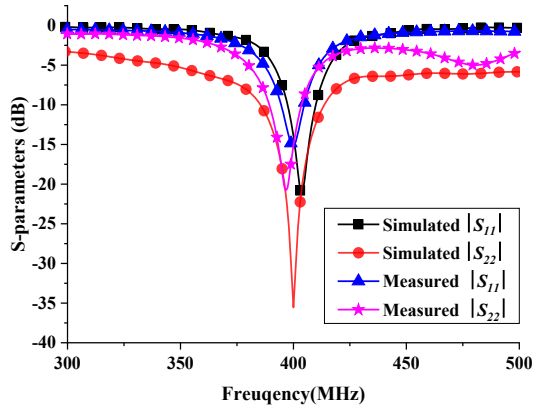

(a)

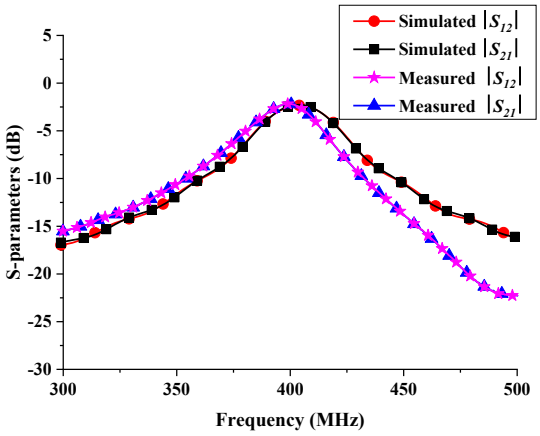

(b)

Fig. 16. The simulated and measured scattering parameters of proposed loops for wireless power transfer (a) reflection coefficient in dB (b) transmission coefficient in dB.

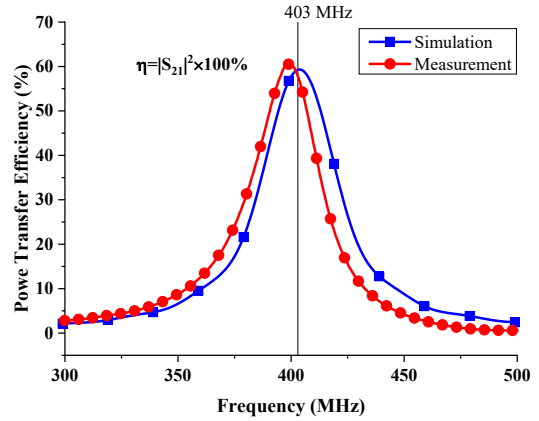

Fig. 17. The simulated and measured power transfer efficiency between the WPT link.

50% within narrow bands from 371 MHz to 394 MHz and from 413 MHz to 420 MHz.

The possible reasons for shifts in the resonant frequency of the system are capacitance tolerance, the depth of the secondary resonator, manufacturing tolerances and variation in environmental conditions.

Comparisons of this design with other works are shown in TABLE III. Maximum source power represents the maximum power that could be supplied to the transmitting loop in consideration of SAR regulations. The table shows that in this work, the PTE is significantly improved at 403 MHz. This is achieved in part by enlarging the dimension of the Rx loop, though its dimension remains small enough to fit within a typical pacemaker. Additionally, the maximum source power available within safe use limits is significantly larger than in other works, which means IMD batteries could be charged faster using this proposed WPT link.

V. RECTIFIER CONFIGURATION

To realize the RF-DC conversion at the receiver side a rectifying circuit is required. Generally, a rectifying circuit consists of an impedance matching network to ensure maximum power is delivered, a rectifying element (diode) to perform RF-to-DC conversion and a DC-pass filter to smooth ripple on the DC output. The voltage doubler rectifier is used in this work since it has a high efficiency and output voltage when compared to that of a simple half-wave rectifier [42].

In consideration of the human safety requirements in Fig. 8, when the power provided to the primary resonator is 55 mW, the calculated SAR value is only 0.692 W/kg, which fully satisfies the safety regulations. In this case, the secondary resonator can receive up to 31.8 mW (≈15 dBm), which can be considered as the source power of the rectifier. A matching circuit is designed to match the load (1.5 kΩ) to the 50 Ω source impedance (the designed secondary resonator is matched for a 50 Ω load impedance) when the input power to the rectifier circuit is 15 dBm. The schematic of the voltage doubler rectifier is shown in Fig. 18. Schottky detector diodes HSMS-286c are selected for the rectifier due to their low-cost.

The rectifier circuit has been simulated and optimized using Advanced Design System (ADS) software. The inductance of the chip inductor (L_1) is 27 nH and the chip capacitances C_1, C_2 and C_3 are 4.7 uF, 4.7 uF and 2.7 pF, respectively. The circuit has been fabricated on FR-4 substrate, as shown in Fig. 19.

The measured and simulated conversion efficiency and the output voltage on the 1.5k Ω load at 403 MHz against input

This article has been accepted for publication in a future issue of this journal, but has not been fully edited. Content may change prior to final publication. Citation information: DOI 10.1109/TAP.2021.3111520, IEEE Transactions on Antennas and Propagation

power are shown in Fig. 20. The measurements were made by attaching an SMA connector to the input end of the rectifier and using an RF signal generator, the voltage on the load was measured using a digital multimeter.

Fig. 20 shows that the output DC voltage increases as the input power increases up to a maximum at which point it becomes a constant value. When diodes are used in the rectifying circuit, the maximum output DC voltage is limited by the reverse breakdown voltage of the diodes. If the input AC voltage is larger than the reverse breakdown voltage of the diodes, the output DC voltage will no longer increase and hence the DC output power will remain constant [44]. The maximum measured conversion efficiency ($\eta_{RF\text{-}DC}$) of the rectifying circuit is 73.2% at 403 MHz when the input power to the rectifier is 17 dBm. The simulated maximum conversion efficiency is 84% when the input power to the rectifier is 15 dBm, however the measurement results still satisfy safety regulations and power delivery requirements for medical devices implanted in the human body. The main reason for this difference is the tolerance of the chip components. The measured conversion efficiency is maintained at over 60% for a variation in rectifier input power from 8 dBm to 18 dBm which is sufficient for low power devices and safe for the human body.

Overall, the measured conversion efficiency and output voltage on the load show good agreement with the simulated results.

VI. Measurement of End-to-End Power Transfer Efficiency

A simplified equivalent schematic diagram of this proposed WPT system is shown in Fig. 21, including the proposed WPT link and the rectifying circuit. To validate the end-to-end power transfer efficiency from RF source power to DC load power, the designed rectifying circuit can be integrated with the Rx resonator directly, as shown in Fig. 22(a). The values of all parameters for Tx, Rx loops and the rectifying circuit are the same as those used in the previous sections.

The measurement setup is illustrated in Fig. 22(b). The SMA100B signal generator from Rohde & Schwarz is used during experiments, which can provide over 25 dBm of input power from 9 kHz to 3 GHz. The transmit loop is directly soldered with an SMA connector and then connected to the signal generator. The RTO2044 oscilloscope from Rohde & Schwarz is used to measure the DC voltage across the load. The receive loop with an integrated rectifying circuit is directly soldered to the oscilloscope differential probe for measurement convenience. The influence of the wires on the measurement can be considered negligible. Both transmit and receive loops with the integrated rectifying circuit were protected by a thin layer of plastic wrap and located appropriately on and within pork mince.

The total system PTE can be found by cascading the two sets of two-port network parameters [43]. The end-to-end power transfer efficiency $\eta_{end\text{-}to\text{-}end}$ of the proposed whole power transfer system can be expressed by

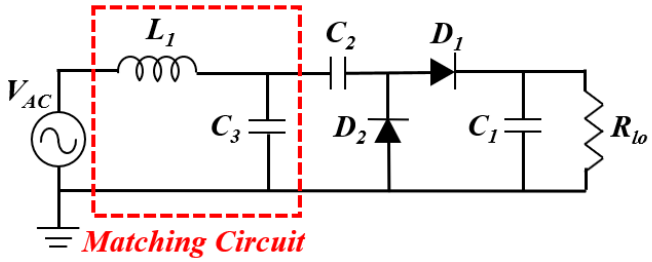

Fig. 18. The schematic of the voltage doubler rectifier.

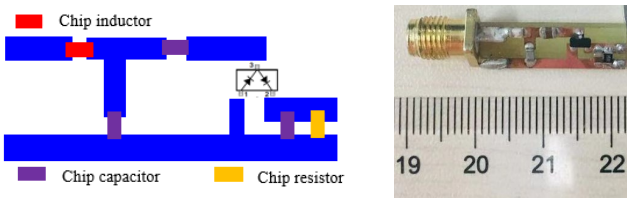

(a) (b)

Fig. 19. (a) Topology of the proposed rectifying circuit; (b) Fabricated rectifying circuit.

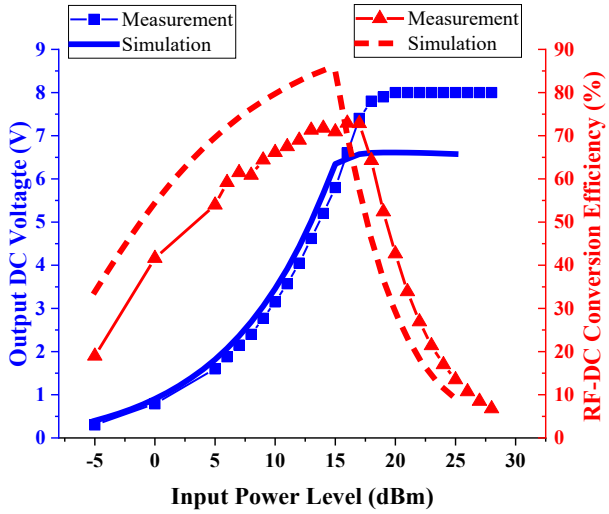

Fig. 20. Measured and simulated RF-DC conversion efficiency and output voltage of the rectifier against input power.

$$\eta_{end-to-end} = \frac{P_{DC}}{P_{transmitting}} = \frac{P_{receiving}}{P_{transmitting}} \times \frac{P_{DC}}{P_{receiving}} = \eta_{RF-RF} \times \eta_{RF-DC} \quad (2)$$

In this case, the theoretical end-to-end wireless power transfer efficiency is approximately 49.8%.

At 403 MHz, the measured DC load voltage (1.5 kΩ), load power and the measured end-to-end PTE between source power and load power are depicted in Fig. 23. As can be seen, the measured DC voltage and load power increase gradually to 8 V and 42.7 mW as the input power rises from -5 dBm (0.32 mW) to 20.5 dBm (112.2 mW) and then remain at 8 V and 42.7 mW despite further increases in input power up to 25 dBm (316.2 mW). The output DC voltage no longer increases due to the reverse breakdown voltage of the diodes. When input power is equal to 19 dBm, a load power of 33.7 mW is achieved. The measured end-to-end PTE climbs slightly from 14% at an input power of −5 dBm to a maximum of 42.4% at an input power of

This article has been accepted for publication in a future issue of this journal, but has not been fully edited. Content may change prior to final publication. Citation information: DOI 10.1109/TAP.2021.3111520, IEEE Transactions on Antennas and Propagation

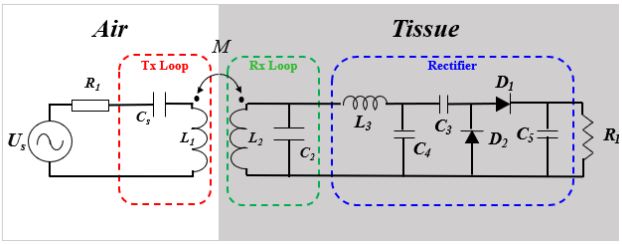

Fig. 21. The equivalent schematic of this proposed WPT system.

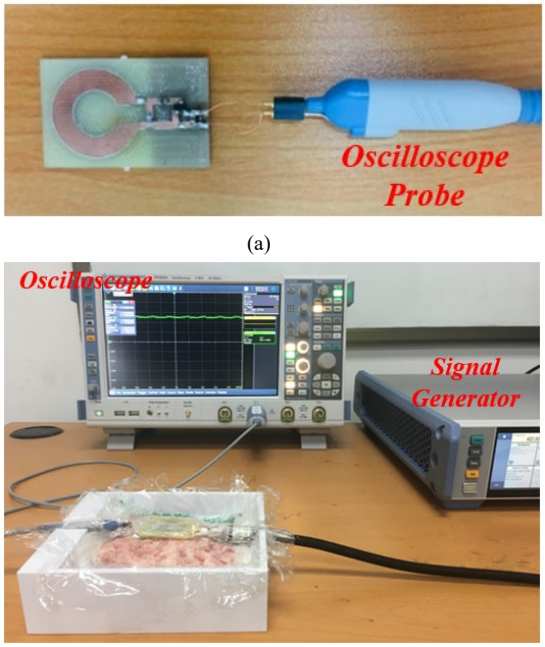

Fig. 22. (a) The proposed Rx loop integrated with rectifying circuit; (b) Measurement setups.

19 dBm (79.4 mW). The end-to-end PTE then declines rapidly to 13.5% as the input power rises from 19 dBm to 25 dBm. The end-to-end PTE is maintained at over 40% over the input power range from 14 dBm (25 mW) to 20 dBm (100 mW). The input power of 20 dBm still satisfies the requirements of the IEEE SAR regulations for the safety of the human body according to Fig. 8. The link power transfer efficiency, RF-to-DC conversion efficiency and end-to-end efficiency of this proposed WPT system is illustrated in TABLE IV.

To investigate the influence of the distance between the Tx and Rx resonators on the end-to-end PTE, trends of measured DC voltage, end-to-end PTE and load power against transfer distance are shown in Fig. 24. The distance between Tx and Rx resonators is varied through 5.5 mm, 6 mm, 10 mm, 15 mm and 20 mm with a 1 mm air gap between the Tx resonator and the surface of the minced pork. The input power is provided at 19 dBm at 403 MHz. The measured DC voltage, end-to-end PTE and load power drop off dramatically as the transfer distance increases. The maximum measured end-to-end PTE is 46.4% at a transfer distance of 5.5 mm, which produces a DC voltage of 7.44 V and load power of 36.9 mW.

Consequently, the measured end-to-end PTE shows good

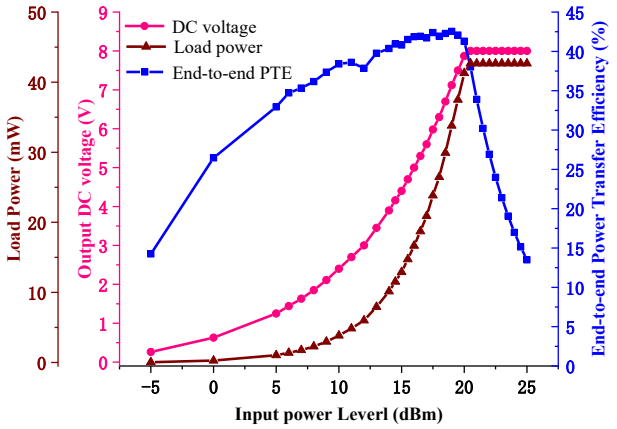

Fig. 23. The measured DC voltage, load power and end-to-end power transfer efficiency against input power at the transfer distance of 6 mm.

TABLE IV. The efficiency of the proposed WPT system at 403 MHz

Quantity	Simulation	Measurement
Link power transfer efficiency of the proposed WPT link ($\eta_{RF\text{-}RF}$)	59.3%	57.9%
RF-to-DC Conversion Efficiency of the rectifying circuit ($\eta_{RF\text{-}DC}$)	84%	73.2%
End-to-end Efficiency of the proposed WPT system ($\eta_{end\text{-}to\text{-}end}$)	49.8%	42.4%

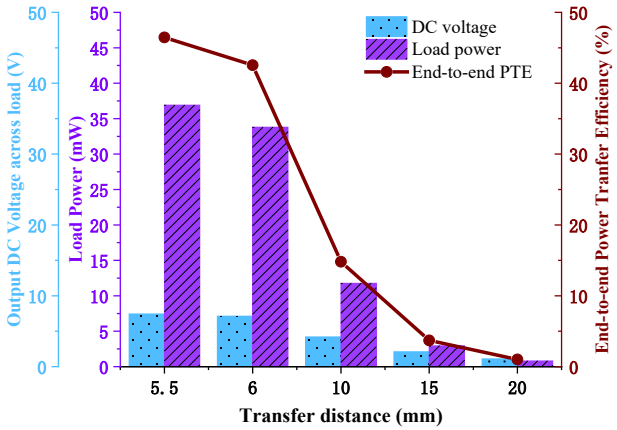

Fig. 24. The measured DC voltage, load power and end-to-end power transfer efficiency against transfer distance at the input power of 19 dBm.

agreement with the calculated efficiency. At 403 MHz, the end-to-end PTE is 42.4% at a transfer distance of 6 mm with a DC voltage of 7.12 V. The obtained load power is 33.7 mW, sufficient for charging pacemakers.

VII. Conclusion

A near-field wireless power transfer system for implantable devices is presented in this paper. It offers good performance in link PTE at 403 MHz. The measured link PTE of the resonators can reach 57.9% at a transfer distance of 6 mm including a 1 mm air gap and 5 mm of body tissues. The measured results show good agreement with the simulated results. In

consideration of the safety of the human body in relation to implanted devices, the SAR value has been evaluated. To satisfy SAR regulations, the maximum transmit power is 159 mW, which is significantly larger than in other works, potentially reducing charging time for pacemaker batteries. A voltage-doubler rectifier is designed for this WPT link to perform the RF-DC conversion; it has a measured conversion efficiency of 73.2%. The measured end-to-end PTE of this system is 42.4% at a transfer distance of 6 mm, from input to primary resonator outside the human body to DC power inside the body. In conclusion, based on its good performance, high PTE, large allowable transmit power and appropriately compact size, this proposed WPT system is a good candidate for the transference of power in applications involving the charging of implantable devices.

ACKNOWLEDGMENT

The authors would like to express their sincere gratitude to CST AG for providing the CST STUDIO SUITE® electromagnetic simulation software package under the China Key University Promotion Program, and Suzhou Municipal Key Lab for Wireless Broadband Access Technologies in the Department of Electrical and Electronics Engineering, Xi'an Jiaotong-Liverpool University, for research facilities.

REFERENCES

[1] R. Xue, K. Cheng and M. Je, "High-efficiency wireless power transfer for biomedical implants by optimal resonant load transformation", *IEEE Transactions on Circuits and System-I: Regular Papers*, vol.60, no.4, pp.867-874, April 2013.

[2] T. Campi, S. Cruciani, F. Palandrani, V. De Santis, A. Hirata, and M. Feliziani, "Wireless power transfer charging system for AIMDs and pacemakers," *IEEE Transactions on Microwave Theory and Techniques*, vol. 64, no. 2, pp. 633-642. Feb. 2016.

[3] G. Xu, X. Yang, Q. Yang, J. Zhao, and Y. Li, "Design on Magnetic Coupling Resonance Wireless Energy Transmission and Monitoring System for Implanted Devices", *IEEE Trans. Applied Superconductivity*, vol. 26. no.4, pp. 4400804, June.2016.

[4] S. Cruciani, T. Campi, F. Maradei and M. Feliziani, "Numerical simulation of Wireless Power Transfer system to recharge the battery of an implanted cardiac pacemaker," *2014 International Symposium on Electromagnetic Compatibility*, Gothenburg, 2014, pp. 44-47, doi: 10.1109/EMCEurope.2014.6930874.

[5] J. Wang, M. Leach, E. G. Lim, Z. Wang and Y. Huang, "Wireless power transfer using resonance coupling for method for implantable applications", *IEEE International Symposium on Antennas and Propagation & USNC/URSI National Radio Science Meeting*, Boston, MA,USA, July , pp.2557-2558, 2018.

[6] K. Na, H. Jang, H. Ma and F. Bien, "Tracking optimal efficiency of magnetic resonance wireless power transfer system for biomedical capsule endoscopy", *IEEE Transactions on Microwave Theory and Techniques*, vol.63, no.1, pp.295-303, Jan 2015.

[7] Y. Cheng, G. Wang, M. Ghovanloo, "Analytical modeling and optimization of small solenoid coils for millimeter-sized biomedical implants", *IEEE Transaction on Microwave Theory and Techniques*, vol.65, no.3, pp.1024-1035, March 2017.

[8] R. Jegadeesan, S. Nag, K. Agarwal, N. V. Thakor and Y. X. Guo, "Enabling wireless powering and telemetry for peripheral nerve implants", *IEEE Journal of biomedical and Health Informatics*, vol. 19, no. 3, pp. 958-970, May 2015.

[9] R. Wu, W. Li, H. Luo; J. K. Sin and C. P. Yue, "Design and characterization of wireless power links for brain-machine interface applications", *IEEE Transaction on Power Electronics*. vol.29, pp. 5462-5471, 2014.

[10] C. Liu, K. T. Zhang, Z. Zhang, C. Qiu, W. Li, and T. Ching, "Wireless power transfer and fault diagnosis of high-voltage power line via robotic bird", *Journal of Applied Physics*, vol.117, no.17, pp. 1-4, 2015

[11] D. H. Tran, V. B. Vu and W. Choi, "Design of a high-efficiency wireless power transfer system with intermediate coils for the on-board chargers of electric vehicles," *IEEE Transactions on power electronics*. vol. 33, no. 1, pp. 175-187, Jan. 2018.

[12] M. Bojarski, E. Asa, K. Colak and D. Czarkowski, "Analysis and control of multiphase inductively coupled resonant converter for wireless electric vehicle charger application," *IEEE Transactions on Transportation Electrification*, vol. 3, no.2, pp. 312-320, June 2017.

[13] K. Hwang, J. Cho, D. Kim, J. Park; J. K. Kwon, S. I. Kwak, H. H. Park and S. Ahn, "An autonomous coil alignment system for the dynamic wireless charging of electric vehicles to minimize lateral misalignment", *Energies*, vol. 10. no.3, pp.315, 2017.

[14] H. Dinis, I. Colmiais and P. M. Mendes, "Extending the limits of wireless power transfer to miniaturized implantable electronic devices", *Micromachines*, vol.8, no.12, pp. 359, Dec 2017

[15] C. Liu, Y. X. Guo, H. Sun and S. Xiao, "Design and safety consideration of an implantable rectenna for far-field wireless power transfer", *IEEE Transactions on Antennas and Propagation*, vol. 62, no. 11, pp.5798-5806, Nov 2014.

[16] G. Vera, A. Georgiadis, A. Collado and S. Via, "Design of a 2.45 GHz rectenna for electromagnetic (EM) energy scavening", *in Proc. IEEE Radio Wireless Symp.*, pp.61-64, 2010.

[17] R. A. Bercich, D. R. Duffy and P.P. Irazoqui, "Far-field RF powering of implantable devices: safety considerations", *IEEE Trans. Biomed. Engerg.*, vol. 60, no. 8, pp. 2107-2112, Aug. 2013.

[18] A. M. Jawad, R. Nordin, S. K. Gharghan, H. M. Jawad and M. Ismail, "Opportunities and challenges for near-field wireless power transfer: A review", *Energies*, vol.10, no.3, 2017.

[19] K. Agrawal, R. Jegadeesana, Y. X. Guo, N. V. Thakor, "Wireless power transfer strategies for implantable bioelectronics", *IEEE Reviews in Biomedical Engineering*, vol.10, pp.136-161, 2017.

[20] C. Xiao, D. Cheng and K. Wei, "An LCC-C compensated wireless charging system for implantable cardiac pacemakers: theory, experiment and safety evaluation", *IEEE Transactions on Power Electronics*, vol.33, no.6, pp.4894-4905, June 2018.

[21] S. C. Tang, T. L. T. Lun, Z. Guo, K-W Kwok and N. J. McDannold, "Intermediate range wireless power transfer with segmented coil transmitters for implantable heart pumps", *IEEE Transactions on Power Electronics*, vol. 32, no.5, pp.3844-3857, May 2017.

[22] Y. Zeng, D. Qiu, X. Meng, B. Zhang and S. C. Tang, "Optimized Design of Coils for Wireless Power Transfer in Implanted Medical Devices," in *IEEE Journal of Electromagnetics, RF and Microwaves in Medicine and Biology*, vol. 2, no. 4, pp. 277-285, Dec. 2018, doi: 10.1109/JERM.2018.2863955.

[23] S. R. Khan and G. S. Choi, "Analysis and optimization of four-coil planar magnetically coupled printed spiral resonators", *Sensors*, vol.16, 2016.

[24] S. A. Mirbozorgi, P. Yeon and M. Ghovanloo, "Robust wireless power transmission to mm-sized free-floating distributed implants", *IEEE Transactions on Biomedical Circuits and Systems*, vol.11, no.3, pp.692-702, June 2017.

[25] M. R. Basar, M. Y. Ahmad, J. Cho and F. Ibrahim, "An improved wearable resonant wireless power transfer system for biomedical capsule endoscope", *IEEE Transaction on Industrial Electronics*, vol. 65, no.10, pp.7772-7781, Oct 2018.

[26] A. S. Y. Poon, S. O Driscoll and T. H. Meng, "Optimal frequency for wireless power transmission into dispersive tissue", *IEEE Transactions on Antennas and Propagation*, vol.58, no.5, pp.1739-1750, May 2010.

[27] Datasheet of pacemakers in Chuang-ling Company, [Online], http://www.chuang-ling.com/product/pdf?id=16.

[28] M. Kod, J. Zhou, Y. Huang, M. Stanley, M. N. Hussein, A. P. Sohrab, R. Alrawashdeh and G. Wang, "Feasibility Study of Using the Housing Cases of Implantable Devices as Antennas," in *IEEE Access*, vol. 4, pp. 6939-6949, 2016, doi: 10.1109/ACCESS.2016.2613968.

[29] "The Thickest and Thinnest Skin on the Body", [Online]. Available The Thickest and Thinnest Skin on the Body | Actforlibraries.org

[30] "IT'IS Foundation – Database at a Glance", [Online]. Available http://www.itis.ethz.ch/itis-for-health/tissue-properties/database/.

[31] J. Wang, M. P. Leach, E. G. Lim, Z. Wang, and Y. Huang. "Investigation of Magnetic Resonance Coupling Circuit Topologies for Wireless Power Transmission". *Microwave Optical Technology Letter*. 2019; 1–9. https://doi.org/10.1002/mop.31803.

[32] J. Wang, M. P. Leach, E. G. Lim, Z. Wang, Z. Jiang, R. Pei, and Y. Huang, "A Conformal Split-ring Loop as a Self-resonator for Wireless Power Transfer," *IEEE Access*, vol. 8, pp. 911-919, 2020.

[33] V. Talla and J. R. Smith, "An experimental technique for design of practical wireless power transfer systems", *IEEE International Symposium on Circuits and Systems, Melbourne VIC, Australia,* pp.2041-2044, 2014.

[34] IEEE Standard for Safety Levels with respect to Human Exposure to Radio Frequency Electromagnetic Fields, 3KHz to 300 GHz, *IEEE Standard C95*. 1-2005, 2005.

[35] M. Mark, T. Björninen, L. Ukkonen, L. Sydänheimo and J. M. Rabaey, "SAR reduction and link optimization for mm-size remotely powered wireless implants using segmented loop antennas," *2011 IEEE Topical Conference on Biomedical Wireless Technologies, Networks, and Sensing Systems*, 2011, pp. 7-10, doi: 10.1109/BIOWIRELESS.2011.5724339.

[36] T. Campi, S. Cruciani, V. De Santis and M. Feliziani, "EMF Safety and Thermal Aspects in a Pacemaker Equipped With a Wireless Power Transfer System Working at Low Frequency," *IEEE Transactions on Microwave Theory and Techniques*, vol. 64, no. 2, pp. 375-382, Feb. 2016,

[37] M. Feliziani and S. Cruciani, "Mitigation of the magnetic field generated by a wireless power transfer (WPT) system without reducing the WPT efficiency," *2013 International Symposium on Electromagnetic Compatibility*, Brugge, pp. 610-615, 2013.

[38] M. Machnoor, E. S. Gámez Rodríguez, P. Kosta, J. Stang and G. Lazzi, "Analysis and Design of a 3-Coil Wireless Power Transmission System for Biomedical Applications," *IEEE Transactions on Antennas and Propagation*, vol. 67, no. 8, pp. 5012-5024, Aug. 2019.

[39] A. Sharma, E. Kampianakis and M. S. Reynolds, "A dual-band HF and UHF antenna system for implanted neural recording and stimulation devices", *IEEE Antennas Wireless Propagation Letters*, vol. 16, pp. 493-496, 2017.

[40] L. Li, H. Liu, H. Zhang and W. Xue, "Efficient wireless power transfer system integrating with metasurface for biological applications", *IEEE Transactions on Industrial Electronics*, vol.65, no.4, pp.3230-3239, 2018.

[41] G. Moti, M. V. D. Paolis, L. Corchia, L. Tarricone, "Wireless resonant energy link for pulse generators implanted in the chest", *IET Microwave, Antenna and Propagation*, vol.11, no.15, pp.2201-2210, 2017.

[42] C. Song, Y. Huang, J. Zhou and P. Carter, "Improved ultrawideband rectennas using hybrid resistance compression technique", *IET Transactions on Antennas and Propagation*, vol.65, no.4, pp. 2057-2062, Feb. 2017.

[43] C. R. Valenta and G. D. Durgin, "Harvesting Wireless Power: Survey of Energy-Harvester Conversion Efficiency in Far-Field, Wireless Power Transfer Systems," in *IEEE Microwave Magazine*, vol. 15, no. 4, pp. 108-120, June 2014.

[44] Robert E. Collin, "Circuit Theory for Waveguiding Systems," in *Foundations for Microwave Engineering*, New York, IEEE, 2001, pp. doi: 10.1109/9780470544662.ch4.

JINGCHEN WANG received the M. Eng degree in Electrical and Information Engineering from Xi'an Jiaotong University, Xi'an, China in 2013 and the Ph.D. in Electrical Engineering and Electronics from University of Liverpool, Liverpool, UK in 2019, respectively.
Dr. Wang is currently a lecturer with the School of Advanced Technology, Xi'an Jiaotong-Liverpool University. Her research interests include wearable antennas, implantable antennas, wireless power transfer, energy harvesting and 5G/5G+ wireless communications. She has been a reviewer of the IEEE TRANSACTIONS ON ANTENNAS AND PROPAGATION, IEEE ACCESS, IEEE TRANSACTIONS ON CIRCUITS AND SYSTEMS I: REGULAR PAPERS, IEEE SENSORS JOURNAL, SENSORS.

ENG GEE LIM received the BEng(Hons) and PhD degrees in Electrical and Electronic Engineering from the UK. Prof. Lim worked for Andrew Ltd, a leading communications systems company in the United Kingdom from 2002 to 2007.
Since August 2007, Prof. Lim has been at Xian Jiaotong-Liverpool University, where he was formally the head of EEE department and University Dean of Research and Graduate studies. Now, he is School Dean of Advanced Technology, director of AI university research centre and also professor in department of Electrical and Electronic Engineering. He has published over 100 refereed international journals and conference papers. His research interests are Artificial Intelligence, robotics, AI+ Health care, international Standard (ISO/IEC) in Robotics, antennas, RF/microwave engineering, EM measurements/simulations, energy harvesting, power/energy transfer, smart-grid communication; wireless communication networks for smart and green cities. He is a charter engineer and Fellow of both IET and Engineers Australia. In addition, he is also a senior member of IEEE and Senior Fellow of HEA.

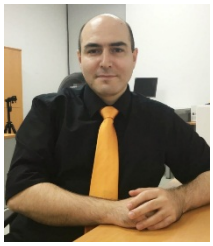

MARK PAUL LEACH received the BEng (Hons) in Communication and Electronic Engineering from the University of Northumbria, UK in 1999 and Ph.D from the same institution in 2005.
Dr. Leach worked as a research associate from 2003 to 2008 in the field of Microwave Holography. From 2008 to 2013 he was employed as a lecturer at Seoul National University of Science and Technology, conducting research into thin films for photovoltaic applications. In 2013 he joined the Department of Electrical and Electronic Engineering at Xi'an Jiaotong Liverpool University; where he is now Deputy Dean of the School of Advanced Technology, his current research interests are in antennas, RF/microwave engineering, EM measurements, energy harvesting, wireless power/energy transfer and wireless communication networks.

ZHAO WANG received the BEng in Electronic and Information Engineering from Xi'an Jiaotong University, China in 2003 and the Ph.D. in Wireless Communication and Electromagnetics from Queen Mary University of London, UK in 2009, respectively.
Dr. Wang has been with the School of Advanced Technology, Xi'an Jiaotong-Liverpool University, where she is currently an associate professor, since 2010. Her research interests are antennas and the optimization algorithms, RF & microwave engineering, energy harvesting and wireless power transfer.

RUI PEI received B.Eng. (Hons.) degrees from Xi'an Jiaotong – Liverpool University and the University of Liverpool in 2015. He received M.Sc. degree (with distinction) from the University of Edinburg in 2016. He is currently working towards the Ph.D. degree from the University of Liverpool.
His research interests include antenna design, wearable antennas, metamaterials, specific absorption rate and body area networks.

ZHENZHEN JIANG received the B.Eng. degree (Hons.) in telecommunication engineering from Xi'an Jiaotong-Liverpool University and the University of Liverpool, in 2016. She is currently pursuing the Ph.D. degree in wireless communications and RF engineering with the University of Liverpool, Liverpool, U.K.
Her research interests include implantable antenna design, simultaneously wireless power and data transfer, energy harvesting, and wireless personal area networks applications.

YI HUANG (S'91 - M'96 - SM'06 – F'20) received BSc in Physics (Wuhan University, China) in 1984, MSc (Eng) in Microwave Engineering (NRIET, Nanjing, China) in 1987, and DPhil in Communications from the University of Oxford, UK in 1994. He has been conducting research in the areas of wireless communications, applied electromagnetics, radar, and antennas since 1987. His experience includes 3 years spent with NRIET (China) as a Radar Engineer and various periods with the Universities of Birmingham, Oxford, and Essex at the UK as a member of research staff. He worked as a Research Fellow at British Telecom Labs in 1994, and then joined the Department of Electrical Engineering & Electronics, the University of Liverpool, UK as a Faculty in 1995, where he is now a full Professor in Wireless Engineering, the Head of High Frequency Engineering Group and Deputy Head of Department. Prof. Huang has published over 350 refereed papers in leading international journals and conference proceedings, and authored Antennas: from Theory to Practice (John Wiley, 2008) and Reverberation Chambers: Theory and Applications to EMC and Antenna Measurements (John Wiley, 2016). He has received many research grants from research councils, government agencies, charity, EU and industry, acted as a consultant to various companies, and served on a number of national and international technical committees and been an Editor, Associate Editor or Guest Editor of five international journals. He has been a keynote/invited speaker and organiser of many conferences and workshops (e.g. WiCom 2006, 2010, IEEE iWAT2010, LAPC2012 and EuCAP2018). He is at present the Editor-in-Chief of Wireless Engineering and Technology, Associate Editor of IEEE Antennas and Wireless Propagation Letters, UK and Ireland Rep to European Association of Antenna and Propagation (EurAAP), a Fellow of IEEE, a Fellow of IET, and a Senior Fellow of HEA.